International Journal of GEOMATE, Feb., 2025 Vol.28, Issue 126, pp.108-115
ISSN: 2186-2982 (P), 2186-2990 (O), Japan, DOI: https://doi.org/10.21660/2025.126.g14166
Geotechnique, Construction Materials and Environment

EFFECTS OF ORTHOGONAL LATERAL LOADING ON ULTIMATE LATERAL PILE LOAD CAPACITY AND LATERAL FLOW BEHAVIOR OF A MODEL PILE

*Thawatwong Phatsak[1] and Warat Kongkitkul[2]

[1,2] Department of Civil Engineering, Faculty of Engineering,
King Mongkut's University of Technology Thonburi, Bangkok, Thailand

*Corresponding Author, Received: 28 Nov. 2024, Revised: 12 Dec. 2024, Accepted: 15 Dec. 2024

ABSTRACT: Previous studies have primarily focused on the effects of unidirectional lateral loading on piles, forming the basis for established design guidelines. However, in practical applications, lateral loads on pile foundations often act in multiple directions. This study examines the behavior of a model single pile subjected to orthogonal lateral loads, specifically analyzing how different loading levels in the x-direction impact the pile's response to subsequent loading in the y-direction. A specially designed bi-directional lateral loading apparatus was used to independently apply loads in the x and y directions, allowing for diverse lateral loading paths. Findings indicate that increasing preloading in the x-direction reduces the ultimate lateral load capacity of the pile under y-direction loading. Additionally, increasing the load in the y-direction while holding the x-direction load constant alters the pile's lateral flow behavior, with these variations diminishing as the y-direction load rises. The p_y-y curve shows a decreasing slope with higher x-direction loads, suggesting a reduction in y-direction soil modulus (E_s). Both the p_y-y and p_x-x curves are affected by loads in the orthogonal direction, highlighting the importance of accounting for preload history and levels when predicting pile performance under multidirectional lateral forces.

Keywords: Bi-directional lateral loading, Pile behavior, Ultimate lateral pile load capacity, Lateral flow characteristics, Sand

1. INTRODUCTION

Previous studies on pile foundations have largely focused on unidirectional lateral loading, investigating soil properties, pile-soil interactions, and load characteristics through model tests [1-6]. These studies have enhanced our understanding of pile behavior under lateral forces caused by wind, wave action, and soil displacement [7]. However, in practical applications, lateral loads on pile foundations often act in multiple directions, which has not been adequately addressed in current research.

Multidirectional lateral loading is particularly significant in structures such as integral abutment bridges, offshore platforms, retaining walls, and high-rise buildings in urban environments. For example, in integral abutment bridges, soil pressures behind abutment walls exert direct lateral forces on foundational piles, which are further influenced by thermal expansion and seismic forces [8-10]. Despite the critical role of multidirectional loads in real-world scenarios, the majority of design guidelines are based on assumptions derived from unidirectional loading conditions, which may lead to overly simplistic and potentially non-conservative designs for such structures.

The p–y method is a widely adopted approach for evaluating pile behavior under lateral loading. It models the relationship between lateral soil resistance (p) and pile deflection (y), providing valuable insights into pile-soil interactions. Mayoral et al. [11] demonstrated how cyclic lateral loading modifies p–y curves in clay due to gap evolution, while Rudolph et al. [12] found that multidirectional loading on large-diameter piles, such as those used in offshore wind turbines, results in greater displacement accumulation compared to unidirectional loading. These findings suggest that traditional p–y curves fail to capture the complexities of multidirectional forces, potentially underestimating their impact. Su and Yan [13] addressed this limitation by proposing a finite element-based p–y model that accounts for multidirectional loading, highlighting significant variations in soil modulus (E_s) and lateral resistance with changing load direction.

Building on these findings, this study aims to deepen the understanding of pile behavior under multidirectional lateral loads. A model single pile was tested using a custom-built bi-directional lateral loading apparatus, which allowed independent application of loads in the x and y directions. This setup enabled detailed analysis of the pile's response to varying loading levels, focusing on the influence of preloading in one direction on subsequent loading in another.

The findings provide critical insights for refining design guidelines to account for multidirectional lateral loading conditions, ensuring greater

reliability, safety, and stability in pile-supported structures subjected to complex real-world forces.

2. RESEARCH SIGNIFICANCE

This study investigates the effects of orthogonal lateral loading on the ultimate lateral pile load capacity and lateral flow behavior of a model pile. Using a custom bi-directional lateral loading apparatus, it examines how preloading in one direction influences the pile's response to subsequent orthogonal loading, focusing on critical parameters such as ultimate load capacity, soil resistance, and lateral flow characteristics. The findings offer valuable insights for improving design guidelines for structures such as offshore platforms, integral abutment bridges, and retaining walls. By addressing the complex interplay of multidirectional forces, this research enhances the safety, reliability, and performance of pile-supported structures and bridges the gap between conventional unidirectional models and real-world multidirectional loading conditions.

3. TEST MATERIALS AND METHOD

3.1 Sand

The soil layer was modeled using KMUTT sand, a type of riverbed sand commonly used in experiments at the Geotechnical Engineering Laboratory of King Mongkut's University of Technology Thonburi (KMUTT) [14-21]. This sand was treated by flushing with tap water to remove impurities, oven-drying it, and sieving to ensure only particles smaller than No. 40 but larger than No. 100 were used. The gradation characteristics, along with the physical and index properties, are illustrated in Fig. 1.

3.2 Pile

A series of 1-g physical model tests were conducted in this study. The prototype concrete pile was 60 cm in diameter and 18 m long. Modeling followed the scaling law [22] with a scaling factor (n). Ensuring similarity in flexural rigidity (EI) between the prototype and modeled piles was crucial. An aluminum pipe (Fig. 2(a)), 3.05 cm in outer diameter, 0.31 cm thick, and 90 cm long, was used. Table 1 compares the characteristics of the prototype and modeled piles. The n values for dimensions are nearly identical, while EI is 17.4, close to the target n=20. Lateral loading was applied at the pile head, and the mobilized bending moment (M) at various locations along the pile length (z) was measured using strain gauges attached to the inside surface of the modeled pile. Due to lateral loading in two directions (x and y axes, Fig. 2(b)), two strain gauges (W and E for the x-axis, N and S for the y-axis) were attached at each z value, forming a full Wheatstone bridge circuit to measure M independently along the x and y axes. M values were measured at ten locations along the length in each direction.

3.3 Test Setup

A concrete container, 100 cm in diameter and 98 cm high, was used, supported by a metal frame acting as a reaction frame. The sand layer was prepared using the air-pluviation method to ensure high uniformity, with a density of approximately 1.55 g/cc. Bi-directional orthogonal lateral loading was applied to the modeled pile using a newly developed lateral loading apparatus installed on the loading frame (Fig. 3). The piston of the precise gear loading machine, controlled automatically by a computer, was connected to a primary steel frame positioned on linear guideways, with a universal joint enabling movement along the y-direction. For loading in the x-direction, a secondary steel frame on another set of linear guideways was connected to a double-action air cylinder with controllable constant pressure. Both the primary and secondary steel frames were designed to accommodate axial load cells for measuring load independently in the y and x directions.

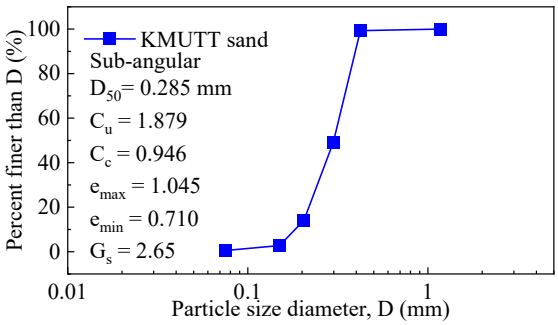

Fig. 1 Gradation, physical, and index properties of KMUTT sand

Table 1 Comparison of characteristics between the prototype concrete pile and the modeled aluminum pile (scaled to n=20) used in the study.

Characteristics	Prototype concrete pile	Modeled Aluminum pile	Target scaling factor	Achieved scaling factor
D	0.60	0.0305	20	19.7
L	18	0.9	20	20
E	20	55		
I	6.362×10^{-3}	2.536×10^{-8}		
EI	1.272×10^{8}	1.395×10^{3}	20^4	17.4^4

D = Diameter (m); L = Length (m); E = Elastic Young's modulus (GPa); I = Moment of inertia (m^4); and EI = Flexural stiffness (Nm^2)

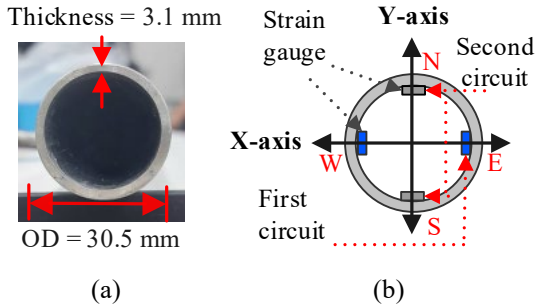

Fig. 2 Dimensions of the modeled aluminum pile and arrangement of strain gauges for measuring bending moments in x and y axes.

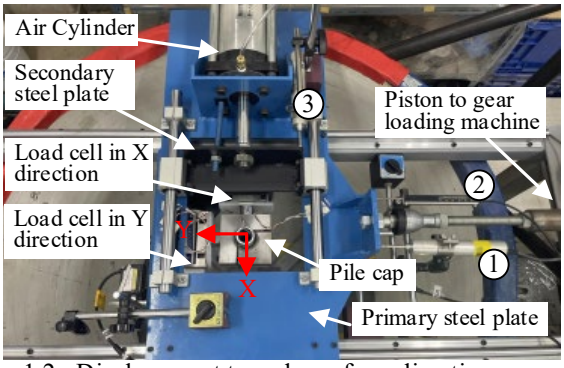

Fig. 3 Newly developed lateral loading apparatus installed on the loading frame.

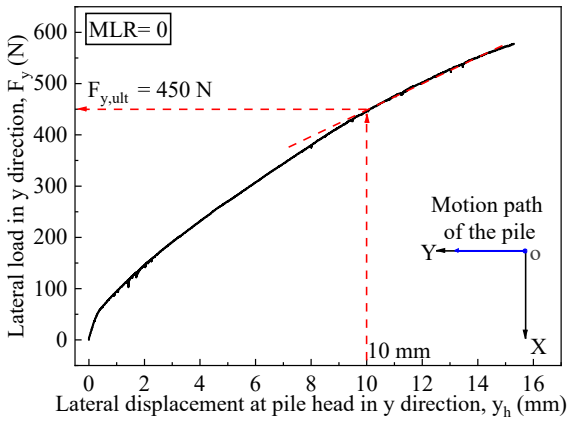

Fig. 4 Lateral load (F_y) vs. lateral displacement at pile head (y_h) by loading in y-direction with preloading in x-direction with MLR=0.

To eliminate the effect of load cell ratcheting when the pile undergoes loading in the orthogonal direction, a miniature linear guide was inserted between each load cell and the steel frame. This ensures that the measured load values are accurate and free from system constraints. Additionally, a specially designed pile cap securely connects to both load cells and the modeled pile. Its curved internal edge where it clamps with the modeled pile prevents activation of bending moments at the pile head, allowing the pile head to rotate freely. For measuring lateral deformation at the pile head, three displacement transducers were used. Two transducers measured lateral deformation in the y-direction: one was connected to the precise gear loading machine for feedback control, and the other was connected to a data logger. The third displacement transducer, connected to a data logger, measured lateral displacement in the x-direction.

3.4 Loading Schemes

In this study, bi-directional loading was applied to the pile head sequentially, first in the x-direction and then independently in the y-direction. Initially, preloading in the x-direction was applied by gradually increasing air pressure at a rate of 1.2 kPa/min until reaching different target loads, after which the pressure was maintained constant (Stage 1). These target loads were defined by various monotonic load ratio (MLR) values, representing the ratio of lateral load at the pile head to the ultimate load under unidirectional loading conditions. The MLR values for preloading in the x-direction were set at 0 (unidirectional), 0.25, 0.50, 0.75, and 1.00. It is worth noting that the actual multidirectional lateral loading scheme in the field may be more complex than the bi-directional loading scheme employed in this study.

4. TEST RESULTS

4.1 Ultimate Lateral Pile Load Capacity

Fig. 4 illustrates the relationship between the lateral load (F_y) and displacement at the pile head (y_h) during lateral loading in the y-direction, with preloading in the x-direction set to MLR = 0. Typically, the ultimate lateral pile load capacity (F_{ult}) of a single pile is determined as the lateral load at the pile head corresponding to a specified lateral pile displacement along the lateral load-displacement curve. In this study, y_h = 10 mm, as suggested by Ni et al. [23] and equivalent to 0.3D where D is diameter [13], was selected to define F_{ult}. The ultimate lateral pile load capacity ($F_{y,ult}$) under loading in the y-direction with MLR = 0 was equal to 450 N, as shown in Fig. 4.

Fig. 5(a) shows the relationship between the lateral load (F_x) and displacement at the pile head (x_h) during preloading in the x-direction for various MLRs in Stage 1. It can be seen that F_x increases with increasing x_h for all the tests, as indicated by o-a_i where i = 1, 2, 3, and 4 in the figure.

The F_x-x_h curves for higher MLRs overlay perfectly over the ones for lower MLRs, showing high repeatability of the test results. Interestingly, in

Stage 2, where F_x is kept constant but y_h is introduced independently, x_h also increases even though F_x is constant, as indicated by a_i-b_i where i = 1, 2, 3, and 4 in the figure. Point b_i corresponds to y_h = 10 mm for respective MLRs.

Moreover, the x_h increment during loading in the y-direction with F_x constant increases with increasing MLR. This evidences the effect of preloading in the x-direction on the displacement in the x-direction when lateral load is exerted in the y direction. This behavior differs from that of an unsupported elastic cantilever cylinder beam subjected to loadings in two lateral orthogonal forces, where x_h and y_h can be independently determined from F_x and F_y with no interaction.

The F_y-y_h relationships under lateral loading in the y-direction while keeping F_x constant for various MLRs are shown in Fig. 5(b). Generally, it can be observed that the F_y-y_h curves for higher MLRs are less stiff than those for lower MLRs. The $F_{y,ult}$ values are 431, 421, 408, and 391 N for MLRs of 0.25, 0.50, 0.75, and 1.00, respectively.

These values are progressively smaller than the $F_{y,ult}$ of 450 N for unidirectional lateral loading where MLR = 0. This behavior indicates that pre-failure directional loading history affects the ultimate lateral pile load capacity. These findings align with the study by Su [24] and Su and Yan [13]

4.2 Lateral Flow Characteristics

Fig. 6 shows the lateral loading paths (F_y-F_x relationships) for various MLRs. It can be seen that F_y is kept zero in Stage 1, while F_x is kept constant in Stage 2. In this figure, at specified F_y values during Stage 2, the corresponding instantaneous lateral displacement vectors (Δy_h:Δx_h) were plotted to present the lateral flow characteristic.

For MLR = 0, all the vectors for various F_y values head in the same direction as the force applied. However, when MLR is more than 0, the vectors deviate from the current direction of the loading path. Comparing at the same MLR, such deviations become less with increasing F_y. But when comparing at the same F_y, the deviations become more with increasing MLR. These behaviors indicate that the lateral flow characteristics depend on both preloading history and load level.

The above-described behaviors can be explained as follows. When the lateral load is applied in the x direction in Stage 1, the passive zone in front of the pile gradually develops, and the margin between the passive zone fully developed at failure and the one currently developed decreases with increasing MLR. Upon applying the lateral load in the y direction, another passive zone in front of the pile also develops, but it is in the y direction. The latter passive zone for the y direction is influenced by the former one for the x direction, causing the Δy_h:Δx_h vectors to head vertically right despite the constant F_x. This influence of the preceding passive zone becomes more pronounced with increasing MLR, causing the direction of the Δy_h:Δx_h vectors to shift further to the right.

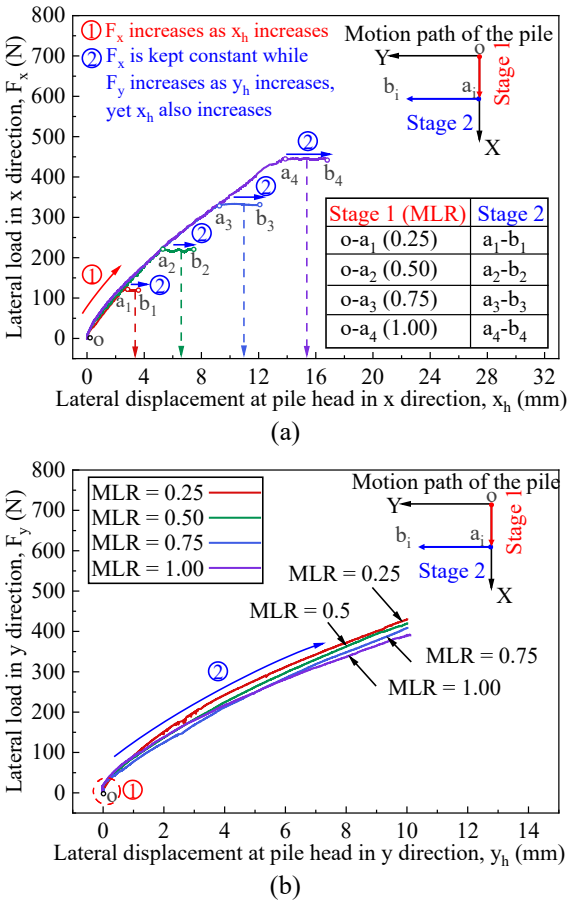

Fig. 5 Lateral load-lateral displacement relationships for various MLRs: (a) F_x-x_h relations during loading in x direction in Stage 1; and (b) F_y-y_h relations during loading in y direction in Stage 2

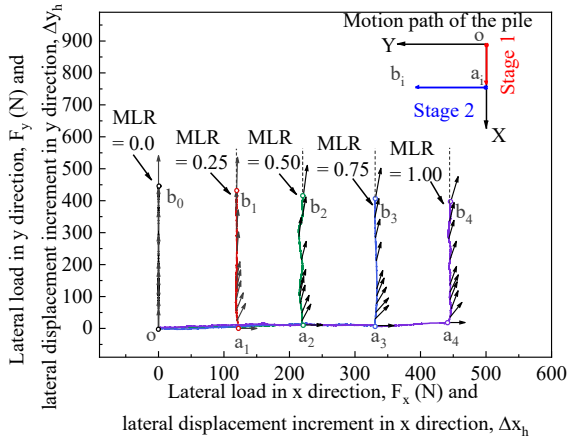

Fig. 6 Lateral loading paths for various MLRs with the corresponding instantaneous lateral displacement vectors (Δy_h:Δx_h)

As lateral loading in the y direction continues, the influence of the latter passive zone for the y direction on the development of soil resistance becomes more significant than that of the former passive zone in the x direction. Consequently, the direction of the Δy_h:Δx_h vectors shifts more upward.

Upon applying bidirectional lateral loading, if the pile head displaces by x_h in the x direction and y_h in the y direction, the total pile head displacement (d_h) can be determined using Equation 1.

$$d_h = \sqrt{x_h^2 + y_h^2} \quad (1)$$

If there is no effect of preloading history in the x direction on the lateral flow characteristics due to subsequent lateral loading in the y direction, the d_h value can be determined based on the F_y-y_h or F_x-x_h relationship alone. Referring to the F_y-y_h relationship shown in Fig. 4, suppose F_x was applied until reaching the specified MLRs; the x_h values corresponding to MLR = 0.25, 0.50, 0.75, and 1.00 are equal to 1.3, 3.8, 6.5, and 9.7 mm, respectively.

Then, suppose that after achieving the above-mentioned MLRs, F_x is held constant while F_y increases to 250 N. Based on the single F_y-y_h or F_x-x_h relationship without considering any interaction, the corresponding y_h = 4.2 mm is obtained. These different x_h values and the same y_h value were then used to calculate the d_h value for different MLRs using Equation 1. Fig. 7 shows the relationships between d_h and MLR obtained as described above. The diagram inset in Fig. 7 depicts the motion path of the pile head according to the assumption above. The flow direction when applying the lateral load in the y direction, while F_x is kept constant, aligns with the direction of F_y (point a to point b_{uni}) as there is no effect of preloading in the x direction.

However, the flow direction measured from the experiment differs from the above assumption. Although F_x remains constant while F_y increases, both x_h and y_h increase, indicating the effect of preloading in the x direction. The flow direction does not align with the currently applied loading direction but follows a curved path (point a to point b_{bi}). When lateral loading in the y direction reaches F_y = 250 N, the corresponding x_h and y_h values for different MLRs were read from Figs. 5(a) and 5(b), respectively. These d_h values were determined and plotted against MLR, as shown in Fig. 7. The d_h values resulting from bidirectional lateral loading are significantly higher than those predicted assuming no effect of preloading in the x direction. Additionally, as MLR increases, the difference between the actual d_h values and those predicted using the single F_y-y_h or F_x-x_h relationship without considering any interaction also increases.

Therefore, the relationship between the load and displacement at the pile head under unidirectional lateral loading cannot accurately predict the pile head displacement under bidirectional lateral loading. The pile head displacement subjected to bidirectional orthogonal loading depends on the preloading history and preloading level. Thus, for actual pile design where it is necessary to predict the lateral deformation at the pile head under bidirectional lateral loading, it is crucial to account for such preloading history and preloading level for accurate deformation prediction.

4.3 Bending Moment

The bending moment (M) in each direction at various depths was measured using strain gauges, with a calibration factor applied to convert bending strain to M. A bending moment diagram along the pile length (M = f(z)) was derived, and a fifth-order polynomial [3, 25] used to fit the M(z) function. Lateral deflection (y) and soil reaction (p) were then calculated from M(z) along the pile depth based on elastic beam theory.

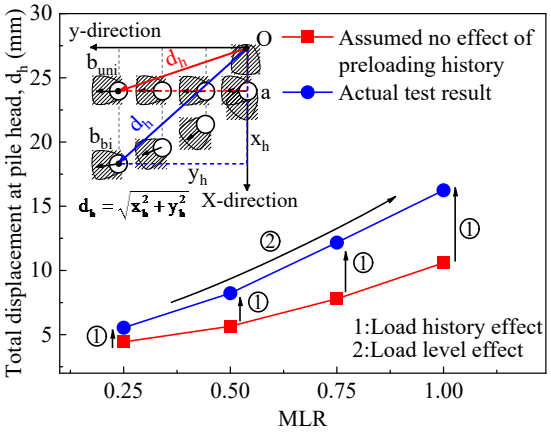

Fig. 7 Comparison of d_h-MLR relationship between the values predicted assuming no effect of preloading in the x direction and the actual values measured from the experiment.

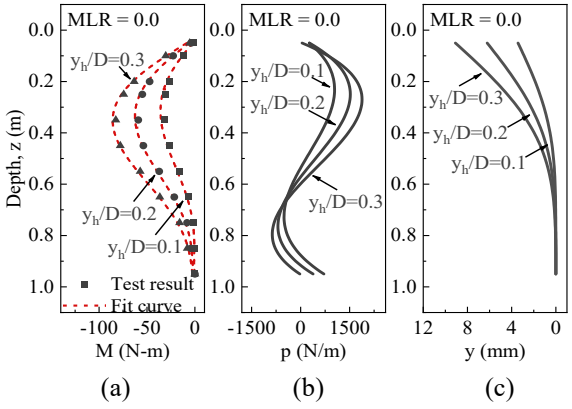

Fig. 8 Comparison of (a) M, (b) p, and (c) y along the pile length for various y_h/D values at MLR = 0

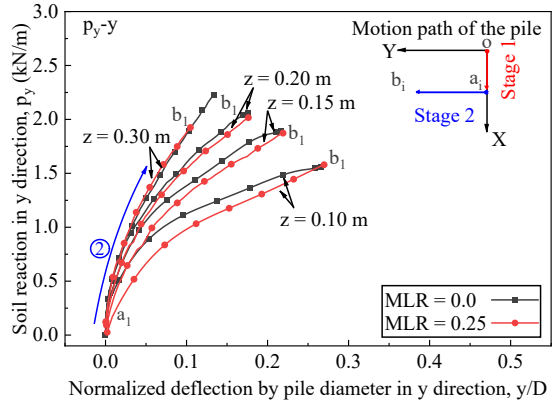

(a)

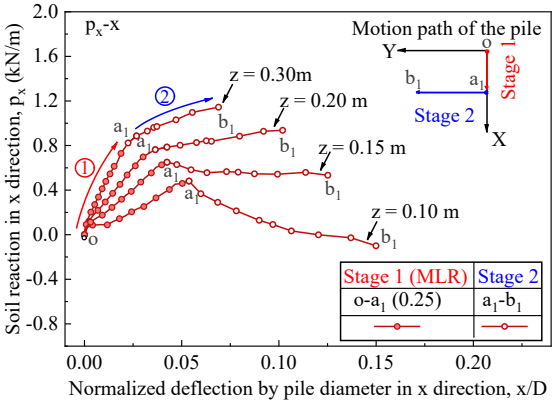

(b)

Fig. 9 p_y-y and p_x-x curves at various pile depths for MLRs = 0 and 0.25

Figure 8 shows the variation of M, y, and p along the pile depth (z) for different lateral y_h values, normalized by pile diameter for MLR = 0. The maximum M values appear at a depth of approximately 10D (z = 0.30 m), where the maximum positive soil reaction also occurs. This depth aligns with the developed passive zone.

4.4 Characteristics of p_x-x and p_y-y along the Pile Depth

In this study, soil reaction and deflection were measured in two directions, with the p_y-y and p_x-x curves illustrating the soil reaction-deflection relationship for the y and x directions, respectively. Depths selected for analyzing p_y-y and p_x-x data range from 0.10 m to 0.30 m, covering the area where the pile encounters passive soil resistance.

For the p_y-y curve at MLR = 0, as pile head displacement increases, the soil reaction rises but at a decreasing rate, as seen in Fig. 9(a). Notably, at z = 0.3 m, the slope of the p_y-y curve is steeper than at 0.10 m, reflecting an increase in soil modulus (E_s) with depth. This pattern is typical for p_y-y curves, where slope indicates E_s, which grows as pile depth increases. The comparison of p_y-y curves between MLR = 0 and MLR = 0.25 in Stage 2 (a_1-b_1), shown in Fig. 9(a), reveals that the slope of the p_y-y curve under unidirectional loading (MLR = 0) is stiffer than under bi-directional loading.

This suggests that the soil modulus (E_s) around the pile decreases when lateral loads are applied to the pile head in two directions.

For the p_x-x curve in Fig. 9(b), the soil reaction in Stage 1 (o-a_1) increases with depth, resembling the behavior of the p_y-y curve under unidirectional lateral loading (MLR = 0), as this stage is unaffected by loads from the other direction. In Stage 2 (a_1-b_1), key behaviors emerge: first, as pile deflection (x) increases, the soil reaction (p_x) decreases at a diminishing rate for depths z = 0.10 m and 0.15 m, indicating that the slope (E_s) of p_x-x curve initially becomes negative but less so as x increases.

Second, the slope of the p_x-x curve gradually becomes less negative with depth, approaching zero around 0.15 m to 0.20 m. Beyond this depth, the slope turns positive at 0.30 m, indicating that p_x increases with x. Notably, the soil reaction (p_x) mobilized at shallower depths during Stage 1 (at point a_1) is transferred to deeper pile depths during lateral loading in the y-direction in Stage 2 (a_1-b_1). This response aligns with the behavior seen in the p-y curve under cyclic lateral loading [26, 27].

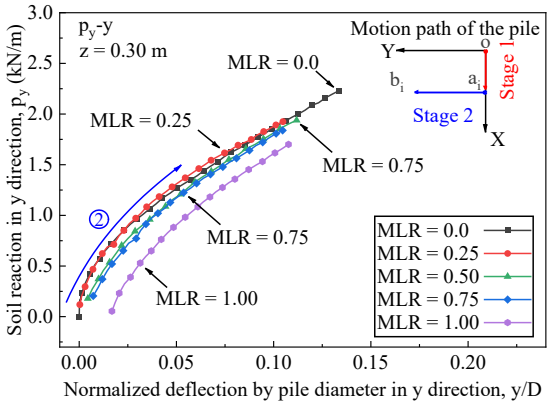

(a)

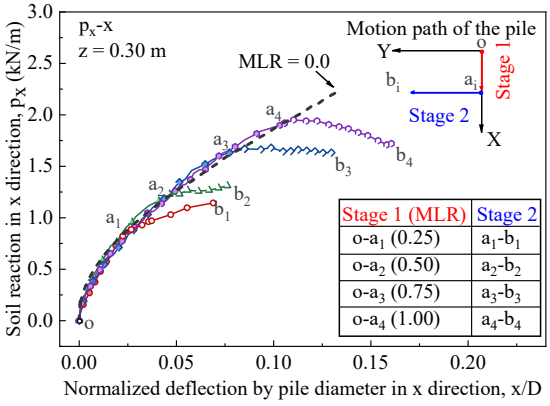

(b)

Fig. 10 p_y-y and p_x-x curves at a pile depth of 0.30 m

4.5 Variations of p_x-x and p_y-y Curves with MLR

Figure 10 shows the relationship between soil reaction and normalized pile deflection for (a) the p_y-y curve and (b) the p_x-x curve. At a depth of 0.30 m, the initial slope (E_{si}) of the p_y-y curve under unidirectional loading is the highest, decreasing as lateral load in the x direction from Stage 1 increases, as seen in Fig. 10(a).

The initial deflection (y) of the p_y-y curve does not start at 0 mm, likely due to a gap between the pile and surrounding soil created by the lateral force in the x direction during Stage 1. Consequently, as force begins to act in the y direction, the pile shifts from its initial position to a new one without resistance from the surrounding soil.

For the p_x-x curves in Stage 2 (a_1-b_1) at a depth of 0.3 m, shown in Fig. 10(b), the soil modulus (E_s) during unidirectional loading is higher than during bidirectional loading, consistent with findings by Su [13]. As the MLR increases, the slope (E_s) gradually decreases and eventually becomes negative. The behaviors described above are due to lateral loading applied in an orthogonal direction, which decreases soil resistance. This effect is similar to that observed in the p_x-x curves in Stage 1 (a_1-b_1) at various depths (Fig. 9(b)).

It is clear that load history affects soil reaction, and when a previous load is applied in an orthogonal direction, this influence intensifies, extending to greater depths under bidirectional loading history. The p_y-y and p_x-x curves under bidirectional orthogonal loading depend on preload history and preload levels. Therefore, the soil modulus (E_s) derived from p-y curves in unidirectional loading cannot accurately represent E_s for bidirectional lateral loading in perpendicular directions.

The test results effectively illustrate the behavior of pile under bidirectional loading, underscoring that the p-y curve from unidirectional lateral loading cannot adequately describe pile response under bidirectional lateral loading.

5. CONCLUSIONS

The following conclusions can be derived:

1. A new lateral loading apparatus capable of independently applying lateral loads in the x and y directions was successfully developed, enabling the application of various load or displacement paths.
2. By increasing the preloading level in the x direction, the ultimate lateral pile loading capacity upon the subsequent lateral loading in the y direction decreases.
3. As the load in the y direction increases while maintaining a constant load in the x direction, the pile's flow characteristics diverge from the expected y direction. This deviation varies with the magnitude of the y directional load increase.
4. The p-y curve becomes less steep as the load in the x direction increases, indicating that higher x-direction loads reduce the y-direction soil modulus (E_s). Both p_x-x and p_y-y curves are affected by loading in the orthogonal direction.

Hence, accurate prediction of both the ultimate lateral pile loading capacity and lateral deformation at the pile head under bidirectional loading requires thorough consideration of preloading history and levels.

6. ACKNOWLEDGMENTS

The authors are grateful to King Mongkut's University of Technology Thonburi (KMUTT) for the financial support granted to this research via The Petchra Pra Jom Klao Ph.D. scholarship under contract Grant No. 2/2565. Thanks are also extended to Mr. Kittipob Charoensook, Miss Chonticha Pimsuk, and Miss Montakan Senalohitfor their help for preparing the test setup.

7. REFERENCES

[1] Brown D.A., Morrison C., and Reese L.C., Lateral load behavior of pile group in sand, Journal of Geotechnical Engineering, Vol. 114, No.11, 1988, pp. 1261-1276.

[2] Ilyas T., Leung C., Chow Y.K., and Budi S., Centrifuge model study of laterally loaded pile groups in clay, Journal of Geotechnical and Geoenvironmental Engineering, Vol. 130, No.3, 2004, pp. 274-283.

[3] Kong L. and Zhang L., Centrifuge modeling of torsionally loaded pile groups, Journal of Geotechnical and Geoenvironmental Engineering, Vol. 133, No.11, 2007, pp. 1374-1384.

[4] Kim Y. and Jeong S., Analysis of soil resistance on laterally loaded piles based on 3D soil–pile interaction, Computers and Geotechnics, Vol. 38, No.2, 2011, pp. 248-257.

[5] Mahdi O.K. and Mahmoud S.A.K., Behavior of pile group subjected to cyclic lateral loading in contaminated soils, International Journal of GEOMATE, Vol. 10, No.21, 2021, pp. 1943-1949.

[6] Gunawan S., Hadsari V., and Wijaya W., Calibration of non-linear to linear soil modulus on pile foundation due to lateral loading, International Journal of GEOMATE, Vol. 25, No.111, 2023, pp. 162-169.

[7] Reese L.C., Cox W.R., and Koop F.D. Analysis of laterally loaded piles in sand,

Conference proceedings, in Offshore Technology Conference. 1974, OnePetro, pp. 474-480.
[8] Faraji S., Ting J.M., Crovo D.S., and Ernst H., Nonlinear analysis of integral bridges: finite-element model, Journal of Geotechnical and Geoenvironmental Engineering, Vol. 127, No.5, 2001, pp. 454-461.
[9] Al-Qarawi A., Leo C., and Liyanapathirana D., Effects of wall movements on performance of integral abutment bridges, International Journal of Geomechanics, Vol. 20, No.2, 2020, p. 04019157.
[10] Bloodworth A.G., Xu M., Banks J.R., and Clayton C.R., Predicting the earth pressure on integral bridge abutments, Journal of Bridge Engineering, Vol. 17, No.2, 2012, pp. 371-381.
[11] Mayoral J.M., Pestana J.M., and Seed R.B., Determination of multidirectional py curves for soft clays, Geotechnical Testing Journal, Vol. 28, No.3, 2005, pp. 253-263.
[12] Rudolph C., Bienen B., and Grabe J., Effect of variation of the loading direction on the displacement accumulation of large-diameter piles under cyclic lateral loading in sand, Canadian Geotechnical Journal, Vol. 51, No.10, 2014, pp. 1196-1206.
[13] Su D. and Yan W., A multidirectional p–y model for lateral sand–pile interactions, Soils and Foundations, Vol. 53, No.2, 2013, pp. 199-214.
[14] Kongkitkul W., Punthutaecha K., Youwai S., Jongpradist P., Moryadee S., Posribink T., Bamrungwong C., and Hirakawa D., Simple dynamic hammer for evaluation of physical conditions of pavement structures, Transportation Research Record, Vol. 2204, No.1, 2011, pp. 35-44.
[15] Kongkitkul W., Chaiyaporn U., Youwai S., and Jongpradist P., Role of geogrids in load transfer of pile-supported embankments, Proceedings of the Institution of Civil Engineers-Ground Improvement, Vol. 165, No.4, 2012, pp. 239-248.
[16] Chantachot T., Kongkitkul W., Youwai S., and Jongpradist P., Behaviours of geosynthetic-reinforced asphalt pavements investigated by laboratory physical model tests on a pavement structure, Transportation Geotechnics, Vol. 8, 2016, pp. 103-118.
[17] Thaothip A. and Kongkitkul W., Strength and deformation characteristics of eps bead-mixed sand, International Journal of GEOMATE, Vol. 13, No.35, 2017, pp. 8-15.
[18] Dararat S., Kongkitkul W., Arangjelovski G., and Ling H.I., Estimation of stress state-dependent elastic modulus of pavement structure materials using one-dimensional loading test, Road Materials and Pavement Design, Vol. 22, No.2, 2021, pp. 245-267.
[19] Punya-in Y. and Kongkitkul W., Effects of temperature on the stress-strain-time behavior of sand under shear, Journal of Testing and Evaluation, Vol. 51, No.2, 2023, pp. 686-705.
[20] Jariyatatsakorn K. and Kongkitkul W., Effects of temperature on strength and time-dependent deformation behaviours of hostun sand under shear, International Journal of GEOMATE, Vol. 24, No.102, 2023, pp. 84-93.
[21] Jariyatatsakorn K., Kongkitkul W., and Tatsuoka F., Prediction of creep strain from stress relaxation of sand in shear, Soils and Foundations, Vol. 64, No.3, 2024, p. 101472.
[22] Wood D.M., Crewe A., and Taylor C., Shaking table testing of geotechnical models, International Journal of Physical Modelling in Geotechnics, Vol. 2, No.1, 2002, pp. 01-13.
[23] Ni P., Mangalathu S., Song L., Mei G., and Zhao Y., Displacement-dependent lateral earth pressure models, Journal of Engineering Mechanics, Vol. 144, No.6, 2018, p. 04018032.
[24] Su D., Resistance of short, stiff piles to multidirectional lateral loadings, Geotechnical Testing Journal, Vol. 35, No.2, 2012, pp. 313-329.
[25] Choo Y.W. and Kim D., Experimental development of the p-y relationship for large-diameter offshore monopiles in sands: Centrifuge tests, Journal of Geotechnical and Geoenvironmental Engineering, Vol. 142, No.1, 2016, p. 04015058.
[26] Rosquoët F., Thorel L., Garnier J., and Canepa Y., Lateral Cyclic Loading of Sand-Installed Piles, Soils and Foundations, Vol. 47, No.5, 2007, pp. 821-832.
[27] Verdure L., Garnier J., and Levacher D., Lateral cyclic loading of single piles in sand, International Journal of Physical Modelling in Geotechnics, Vol. 3, No.3, 2003, pp. 17-28.